Korean J. Chem. Eng., **28**(12), 2242-2249 (2011)
DOI: 10.1007/s11814-011-0122-5

Modeling and simulations of a reformer used in direct reduction of iron

Abdelhamid Ajbar†, Khalid Alhumaizi, and Mustafa Soliman

Department of Chemical Engineering, King Saud University, P. O. Box 800, Riyadh 11421, Saudi Arabia
(*Received 26 February 2011 • accepted 5 May 2011*)

Abstract−This paper presents a detailed modeling and simulations of a reformer unit used in the direct reduction of iron (DRI) process. A one-dimensional heterogeneous model for the catalyst tubes which takes into account the intraparticle mass transfer resistance was developed, while the furnace was modeled with bottom firing configuration. Validation against data from a local iron/steel plant showed satisfactory results. The performance variables of the unit were the process gas temperature, wall temperature and conversions of hydrogen, methane and carbon dioxide. The profiles of these output variables along the distance were calculated. The effect of operating parameters such as inlet temperature, natural gas flow rate and gas composition was also determined.

Key words: Direct Reduction of Iron, Reformer, Modeling, Simulation, Performance

INTRODUCTION

The direct reduction process has gained growing importance in the last decades as a source of metallic units for electric arc furnaces used for the production of steel. Midrex technology is the most important DRI process and consists of around 58% of the world total DRI production [1]. In a Midrex process, natural gas is used to manufacture the reducing gas in a reforming process. The Midrex reformer is a bottom-fired box-type furnace with the structure of a straight-flow, co-current type heat exchanger. Conventional steam reformers have been in use in various industries such as ammonia production and methanol plants. However, the production of syngas for reducing iron ores in a Midrex process differs from conventional steam reformers in a number of ways [2-5]: (1) The steam in a Midrex plant is not supplied by a steam generation unit but is provided by the steam content of recycled off gas stream from the furnace; (2) the Midrex reformer operates at lower pressures of 2-3 atm compared to pressures of 20-40 atm in a conventional steam reformer; (3) the Midrex reformer operates at low stoichiometric ratio of oxidant to carbon compared to conventional steam reformers; (4) the content of carbon dioxide in the process feed gas in a Midrex reformer is higher than most conventional steam reformers which increases the risk of carbon deposit.

The mathematical modeling of conventional steam reformers used in chemical and petrochemical industries has been studied well in the literature [6-17]. Various models with different degrees of complexity were used for the design and simulation of these units. These models range from one-dimensional heterogeneous models to two dimensional models [9,15,16]. It is also known that the heat transfer from the furnace to catalyst tubes highly affects the performance of the reactor. Different furnace designs are also available in the literature [18-20].

The modeling of reformers used in direct reduced iron plants has not received similar attention in the literature. Murty and Murthy [20], and Selcuk et al. [22], for instance, used the flux method for radiative transfer [18] to develop models for reformer furnaces. One notable contribution is the work of Farhadi et al. [2] who carried out a detailed one-dimensional heterogeneous model for the Midrex reformer. In a recent study, Shayegan et al. [5] developed a two-dimensional heterogeneous model for the reformer. The authors presented arguments for the need to account for temperature gradients in radial dimension for their studied unit. These include low Reynolds number and low tube length to diameter ratio.

In this paper, a one-dimensional heterogeneous model for the catalyst tubes which takes into account the intraparticle mass transfer resistance is developed for the reformer. The furnace is modeled with bottom firing configuration. Besides its relative simplicity, the choice of one-dimensional model is based on the recent work of Shayegan et al. [5], who concluded that the quality of predictions of the two dimensional model depended strongly on fitted correlations for wall to fluid heat transfer. They also reported that one-dimensional models had better predictions for flue gas temperatures. Moreover, the lack of any radial measurements for the unit under study limits the usefulness of any two dimensional model. Another worthy difference in this work is the choice of kinetics. Previous studies [2,5] used the simple first-order kinetic model of Akers and Camp [23] for which an analytical solution is available for the effectiveness factor, whereas this work uses a more rigorous Langmuir-Hinshelwood type of kinetics [7] for which a numerical solution for the effectiveness factors is needed.

REACTION KINETICS

The kinetic rate expressions considered in this project are those developed by Xu and Froment [7], based on Langmuir-Hinshelwood (Hougen-Watson) approach using a commercial catalyst (Holder Topsoe Ni/Mg Al_2O_4 spinel) in an integral flow reactor. Xu and Froment [7] have taken into consideration the main steam reforming reactions together with the water-gas shift reaction:

$$CH_4+H_2O \leftrightarrow CO+3H_2 \quad (1)$$

†To whom correspondence should be addressed.
E-mail: aajbar@ksu.edu.sa

$$CO+H_2O\leftrightarrow CO_2+H_2 \quad (2)$$

$$CH_2+2H_2O\leftrightarrow CO_2+4H_2 \quad (3)$$

The kinetics of the dry reforming reaction

$$CH_4+CO_2\leftrightarrow 2CO+2H_2 \quad (4)$$

are negligible with respect to the steam reforming reactions (reactions 1 and 3). CO_2 mainly hinders the forward reactions (2) & (3). The authors [7,24] also used an adsorption-desorption mechanism model consisting of 13 steps and reached the following rate equations:

$$r_1=k_1\left(\frac{P_{CH_4}P_{H_2O}}{P_{H_2}^{2.5}}-\frac{P_{H_2}^{0.5}P_{CO}}{K_1}\right)/DEN^2 \quad (5)$$

$$r_2=k_2\left(\frac{P_{CO}P_{H_2O}}{P_{H_2}}-\frac{P_{CO}}{K_2}\right)/DEN^2 \quad (6)$$

$$r_3=k_3\left(\frac{P_{CH_4}P_{H_2O}}{P_{H_2}^{3.5}}-\frac{P_{H_2}^{0.5}P_{CO_2}}{K_1K_2}\right)/DEN^2 \quad (7)$$

with

$$DEN=1+k_{CO}P_{CO}+k_{H_2}P_{H_2}+k_{CH_4}P_{CH_4}+\frac{k_{H_2O}P_{H_2O}}{P_{H_2}} \quad (8)$$

where P_i is the partial pressure of component i. The expressions for reaction rate constants k_1, k_2 and k_3, absorption constants k_{CO}, k_{H_2O}, k_{CH_4} and k_{H_2}, and the equilibrium constants K_1 and K_2 are summarized in Table 1.

The rate of disappearance and formation of CH_4 and CO_2 (taken as key components) is given by:

$$R_{CH_4}=r_1+r_3,\ R_{CO_2}=r_2+r_3 \quad (9)$$

Let the conversions of methane and carbon dioxide be defined by:

$$x_{CH_4}=(n_{CH_4,f}-n_{CH_4})/n_{CH_4,f} \quad (10)$$

$$x_{CO_2}=(n_{CO_2}-n_{CO_2,f})/n_{CH_4,f} \quad (11)$$

Stoichiometric relations in terms of x_{CH_4}, x_{CO_2} can be written as follows:

$$n_{CH_4}=n_{CH_4,f}-x_{CH_4}n_{CH_4,f} \quad (12)$$

$$n_{H_2O}=n_{H_2O,f}-(x_{CH_4}+x_{CO_2})n_{CH_4,f} \quad (13)$$

$$n_{CO}=n_{CO,f}+(x_{CH_4}-x_{CO_2})n_{CH_4} \quad (14)$$

$$n_{CO_2}=n_{CO_2,f}+x_{CO_2}n_{CH_4,f} \quad (15)$$

Table 1. Kinetic parameters rate constants [7]

Parameter	Value
k_1	$9.49\times10^{15}\exp(-240.1/RT)$
k_2	$4.39\times10^{6}\exp(-67.13/RT)$
k_3	$2.29\times10^{15}\exp(-243.9/RT)$
k_{CO}	$8.23\times10^{-5}\exp(-70.65/RT)$
k_{CH_4}	$6.65\times10^{-4}\exp(38.28/RT)$
k_{H_2O}	$1.77\times10^{5}\exp(-88.68/RT)$
k_{H_2}	$6.12\times10^{-9}\exp(82.9/RT)$
K_1	$\exp(-26830.0/T+30.114)$
K_2	$\exp(4400/T-4.036)$

$$n_{H_2}=n_{H_2,f}+(3x_{CH_4}+x_{CO_2})n_{CH_4,f} \quad (16)$$

$$n_T=n_{T,f}+2x_{CH_4}n_{CH_4,f} \quad (17)$$

It is therefore possible to express the number of moles n_i of any component i in the reacting mixture, as well as the total number of moles n_T, in terms of molar feed rates and the conversions of methane and carbon dioxide.

MODEL DEVELOPMENT

1. Model Assumptions

The following are the main assumptions used for the development of the reformer model:

- The reactor is at steady state.
- Radial distribution of the temperature and the concentration of the different components inside the reactor are uniform (i.e., one-dimensional model).
- Heat and mass diffusions in the longitudinal directions are negligible considering the very high gas velocity at which the reactor is operated (i.e., axial dispersion is negligible).
- Ideal behavior is assumed for the gases.
- Mass and heat transfer resistances between the fluid and the particle surface are negligible.

2. Model Equations

A one-dimensional heterogeneous model is used to describe the catalyst tube, which takes into account only the intraparticle mass transfer resistance. One reformer tube performance is assumed to be representative of any other tube, by assuming the feed gas to be distributed equally among the reformer tubes, and that heat flux passing through each tube wall is the same regardless of the location of the tube inside the furnace with respect to the location of the burners.

3. Reactor Equations

The material, energy and momentum balance equations can be written as follows:

$$dx_{CH_4}/dl=A\rho_\theta\eta_{CH_4}R_{CH_4}/n_{CH_4,f} \quad (18)$$

$$dx_{CO_2}/dl=A\rho_\theta\eta_{CO_2}R_{CO_2}/n_{CH_4,f} \quad (19)$$

$$dT/dl=\frac{1}{C_pU_s}\left\{\rho_\theta\Delta H_1\eta_{CH_4}(r_1+r_2)+\rho_\theta\Delta H_2\eta_{CO_2}(r_2+r_3)+4\frac{U}{dt_i}(T_S-T)\right\} \quad (20)$$

$$\frac{dP_T}{dl}=f(G^2/\rho_g d_P) \quad (21)$$

T is the temperature of the reacting mixture, T_s the temperature of inner tube skin, P_T the total pressure along the reformer, A the reformer tube cross sectional area, ρ_θ the bulk density of the catalyst, η_{CH_4} and η_{CO_2} are the effectiveness factors associated with the reactions of CH_4 and CO_2, respectively, dt_i the internal diameter of the reformer tubes, u_s the superficial gas velocity and G is the gas mass velocity. The heat transfer coefficient U needed in the energy balance equation (Eq. (20)) is calculated using the correlation developed in [8,24]. The Ergun correlation is used to calculate the friction coefficient f in the momentum balance Eq. (21) for large Reynolds number:

$$f=1.75\frac{1-\varepsilon}{\varepsilon^3} \tag{22}$$

where ε is the bed void fraction.

4. Catalyst Particle Equations

The catalyst pellets are assumed to be a slab with a characteristic length l_c. The material balance equations for the catalyst pellet take the following form:

$$d^2P_{CH_4,p}/d\omega^2 = R_{CH_4}RTl_c^2/D_{CH_4,e} \tag{23}$$

$$d^2P_{CO_2,p}/d\omega^2 = -R_{CO_2}RTl_c^2/D_{CO_2,e} \tag{24}$$

with the boundary conditions,

$$P_{CH_4,p}=P_{CH_4,s} \;\&\; P_{CO_2,p}=P_{CO_2,s} \text{ at } \omega=1.0 \tag{25}$$

$$\frac{dP_{CH_4,p}}{d\omega}=\frac{dP_{CO_2,p}}{d\omega}=0 \text{ at } \omega=0 \tag{26}$$

$P_{i,p}$ and $P_{i,s}$ designate, respectively, the partial pressure of component i in catalyst particle and on catalyst particle surface, ω the dimensionless coordinate of the catalyst pellet and $D_{i,e}$ is the effective molecular diffusivity of component i. The slab is assumed to be isothermal while external mass and heat transfer resistances are assumed negligible. The physico-chemical parameters such as viscosity, thermal conductivity, molecular diffusivities, are obtained using standard correlations [24,25].

5. Modeling of the Furnace

One type of firing will be considered, the bottom fired furnace. Roesler [18] introduced the two flux model for the one-dimensional furnaces. The model is capable of taking into account the radiative heat along and normal to the gas flow. We will adopt in this work the Roesler model that was modified by Filla [26] to take the following form:

$$\frac{d^2E_1}{dl^2}=\alpha_1\{\beta(E_1-\sigma\psi T_g^4)+\varepsilon_i a_i(E_1-\sigma\psi T_{t,0}^4) + \varepsilon_r a_r((1-\psi)E_1-\psi E_2)\} \tag{27}$$

$$\frac{d^2E_2}{dl^2}=\alpha_2\{\varepsilon_i a_i(E_2-\sigma(1-\psi)T_{t,0}^4)+\varepsilon_i a_r(\psi E_2-(1-\psi)E_1)\} \tag{28}$$

with the following boundary conditions:

At l=0,

$$\frac{1}{\alpha_1}\frac{dE_1}{dl}=-\frac{1}{\alpha_2}\frac{dE_2}{dl}=\frac{\varepsilon_r}{2-\varepsilon_r}\{(1-\psi)E_1-\psi E_2\} \tag{29}$$

At l=L,

$$-\frac{1}{\alpha_1}\frac{dE_1}{dl}=\frac{1}{\alpha_2}\frac{dE_2}{dl}=\frac{\varepsilon_r}{2-\varepsilon_r}\{(1-\psi)E_1-\psi E_2\} \tag{30}$$

E_1 and E_2 are, respectively, the grey and clear gas component heat gas flux, T_g the temperature of furnace gas, $T_{t,o}$ the outer tube surface temperature, σ the Stefan-Boltzmann constant, ψ the band radiation fraction, β the absorption coefficient and ε_g, ε_t are, respectively, the emissivities of the flue gas, refractory slab and tube wall. The other parameters appearing in Eqs. (27)-(30) are defined in the nomenclature. In this model, it is assumed that the gas emissivity can be approximated by

$$\varepsilon_g=\psi\{(1-\exp(-BL^-/2)\} \tag{31}$$

where L^- is the beam length and

$$\alpha_1=\beta+a_t+a_r,\ \alpha_2=a_t+a_r \tag{32}$$

where a_r and a_t are, respectively, the refractory furnace area and the tube side furnace area to furnace free volume half ratio. The refractory temperature T_r is given by:

$$T_r=\left(\frac{E_1+E_2}{\sigma}\right)^{1/4} \tag{33}$$

The differential heat balance on the flue gas stream takes the following form:

$$G_gC_g\frac{d[T_g-F(T^*-T_{g,0})]}{dl}=2\beta[E_1-\psi E_g] \tag{34}$$

where G_g is the process flue gas mass velocity, T* the adiabatic flame temperature, F the fraction of the fuel burned along the reformer and E_g is the gas emissive powers in side fired furnaces. The flue gas inlet temperature $T_{g,0}$ is given by

$$T_{g,0}=\left[\frac{E_{1,0}}{\sigma\psi}\right]^{1/4} \tag{35}$$

where $E_{1,0}$ is the value of E_1 at the gas inlet. The heat transfer by radiation to the reformer tubes is given by:

$$Q_r=2\varepsilon_i a_t(E_r-E_t)V \tag{36}$$

where E_t is the tube emissive powers in side fired furnaces, $E_r=\sigma T_r^4$ and V is the free volume of the reformer.

NUMERICAL SOLUTION STRATEGY

The heat transfer equations describing the furnace can be decoupled from those describing the reaction in the reformer tubes by assuming values of the outer wall temperature profile of the reformer tubes, then carrying out consecutive iterations between the furnace equations and the tube equations until the two iterations match. For the bottom-fired furnace, the differential equations describing the heat transfer in the furnace are discretized by the orthogonal collocation method using a cubic polynomial leading to simultaneous non-linear algebraic equations, which are solved by the subroutine ZSPOW of the IMSL (International Mathematical and Statistical Library) which is based on discretized Newton method. On the other hand, using the assumed wall temperature profile, the four differential equations describing the reformer tubes are solved by a fourth-order Runge-Kutta routine with variable step size, and then iterations are performed to obtain the correct wall temperature. At every location along the reactor the effectiveness factors for the CH_4 and CO_2 have to be calculated. For this purpose, the modified collocation method developed by Soliman [27] is used. The effectiveness factors are calculated using the following formulas:

$$\eta_{CO_2}=\left[2.0\times\int_{P_{CO_2,C}}^{P_{CO_2,S}}R_{CO_2}(P_{CH_4,p},P_{CO_2,p})\frac{dP_{CO_2,p}}{C_1}\right]^{1/2}/R_{CO_2,S} \tag{37}$$

$$\eta_{CH_4}=\left[2.0\times\int_{P_{CH_4,C}}^{P_{CH_4,S}}R_{CH_4}(P_{CH_4,p},P_{CO_2,p})\frac{dP_{CH_4,p}}{C_2}\right]^{1/2}/R_{CH_4,S} \tag{38}$$

With

$$C_1 = RT\frac{l_c^2}{D_{CO_2,e}},\quad C_2 = RT\frac{l_c^2}{D_{CH_4,e}} \tag{39}$$

Some model parameters were needed to be tuned in order to fit the plant data. These include the effectiveness factors for carbon dioxide (Eq. (37)) and methane (Eq. (38)) as well as the heat transfer coefficient. After obtaining the center pressures, it is required to have a relation between the pressures of CH_4 and CO_2 at any position inside the catalyst particle in order to obtain the integrals in equations (Eq. (37)) and (Eq. (38)). This relation is obtained by linear interpolation between the center and surface pressures to get:

$$\frac{P_{CO_2,p} - P_{CO_2,S}}{P_{CH_4,p} - P_{CH_4,S}} = \frac{P_{CO_2,c} - P_{CO_2,S}}{P_{CH_4,c} - P_{CH_4,S}} \tag{40}$$

RESULTS AND DISCUSSION

The simulations were carried out using the reformer design and operating parameters presented in Tables 2 and 3. First, a validation study was carried out using plant data from a local iron/steel plant. Table 4 summarizes the comparison between model predictions and plant data for exit conditions in the reformer. The available plant data are the process temperature and the dry composition of the process gas. Process gas temperature shows excellent fit. As for dry composition, it can be seen that while the compositions of H_2 and CO show very good fit, those of CO_2 and CH_4 show some deviations. The model predicts that too much methane is steam reformed, while the mole fraction of carbon dioxide is larger. These discrepancies could be due to the chosen kinetics and also to the tuning of the effectiveness factors. Moreover, given the small values of the composition themselves, measurement errors could also contribute to these deviations.

Table 2. Nominal values of design parameters of reformer

Parameter	Value
Number of tubes	521
Inside tube diameter (m)	0.2
Tube thickness (m)	0.024
Tube length (m)	7.9
Catalyst particles characteristic length (m)	0.0038
Catalyst pellets bulk density (kg/m^3)	250
Catalyst pore radius (A)	80
Tortosity	2.74

Table 3. Nominal values of operating parameters of reformer

Parameter	Value
Natural gas flow rate to reformer (10^3Nm^3/hr)	22.37
Fraction of methane in natural gas (%)	95
Total pressure (atm)	2.46
Temperature (K)	822.2
H_2O/CH_4	0.44
H_2/CH_4	2.46
CO_2/CH_4	0.54
N_2/CH_4	0.17
CO/CH_4	1.26

Table 4. Comparison between plant data and model predictions at the reformer exit conditions

Parameter	Model predictions	Plant data
Process gas exit temperature (K)	948	945
Composition of dry process gas (%)		
H_2	57.0	57.3
CO	36.1	36.3
CO_2	5.2	3.5
CH_4	0.3	1.2
N_2	1.4	1.7

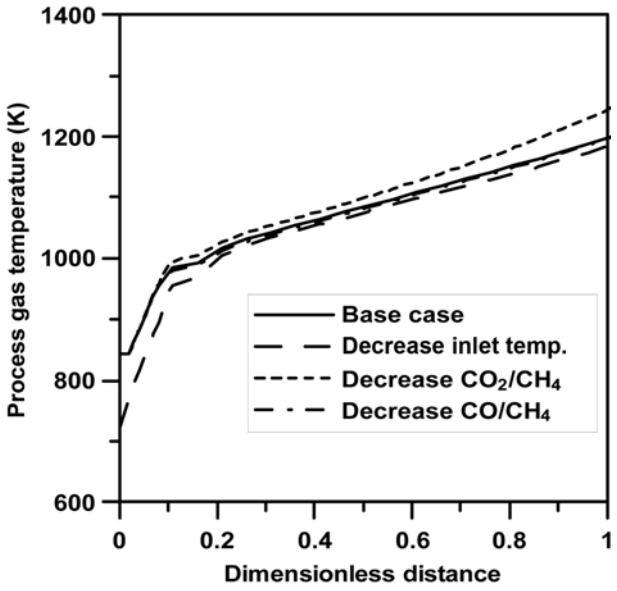

Fig. 1. Variations of process gas temperature and effect of some operating parameters.

Fig. 1 shows the profiles of process gas temperature. An increase in the gas temperature along the distance is expected since the heat from fuel is enough to sustain the increase in the temperature. The profiles of both the wall temperature and the flue gas temperature show, on the other hand, a non monotonic behavior (Figs. 2(a)-(b)). The profiles are plotted for the four collocation points only (explaining the non smoothness of the profiles). Initially, the reaction rates are small, but they keep increasing along the distance causing a rise in both wall and flue gas temperatures. However, since the reaction is endothermic, the heat removal increases along the distance, which causes a decrease in the temperatures.

Figs. 1 and 3 show some sensitivity analysis for the effect of key operating parameters. A decrease in the inlet temperature (from 822.21 to 750 K) causes evidently a decrease in the process gas temperature (Fig. 1). A decrease in the ratio of CO_2/CH_4 (from 0.54 to 0.35) causes a less extent of dry reforming, which leads to a decrease in the heat needed for reforming and therefore causing an increase in the process gas temperature (Fig. 1). A decrease in the ratio of CO/CH_4 (from 1.26 to 1.00) pushes the reactions to occur in the forward direction, and since the reactions are endothermic, this will cause a decrease in the gas temperature.

Fig. 3 shows that an increase in the flow rate of methane (from

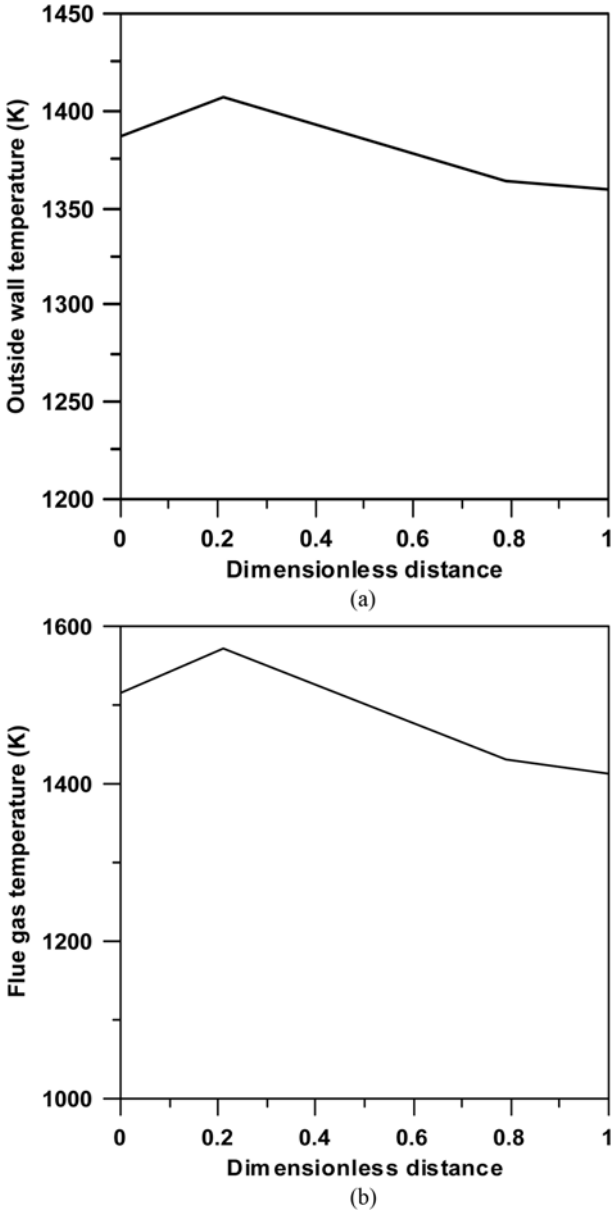

Fig. 2. (b) Variations of: (a) outside wall temperature; (b) flue gas temperature with dimensionless distance at the collocation points.

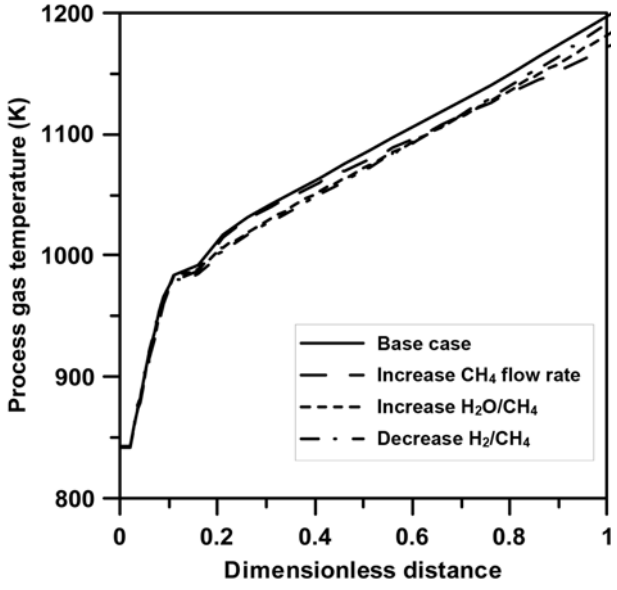

Fig. 3. Variations of process gas temperature and effect of some operating parameters.

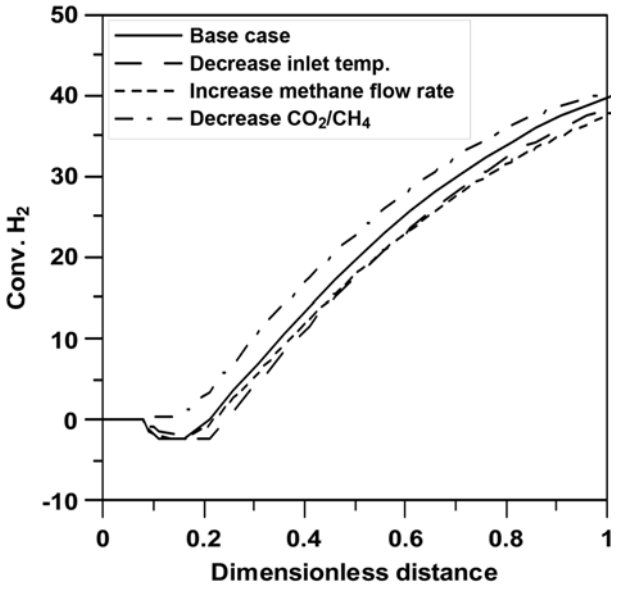

Fig. 4. Variations of hydrogen conversion and effect of some operating parameters.

2.07 kmol/h to 2.33 kmol/h) evidently decreases the gas temperature rise for a given constant heat. The increase in the ratio of H_2O/CH_4 (from 0.43 to 0.70) causes more steam reforming and therefore more heat required for the reaction, and this will ultimately reduce the process gas temperature. On the other hand, the effect of a decrease in the ratio of H_2/CH_4 (from 2.45 to 1.8) causes more reforming and this will cause a reduction in the gas temperature.

The variations of conversions of H_2, CO_2 and CH_4 along the distance are shown in Figs. 4-9. It can be seen that hydrogen conversion increases with distance as a natural result of reforming. Fig. 4 shows that a decrease in the inlet temperature causes less reforming and therefore leads to a decrease in the conversion compared to the nominal case. An increase in the methane flow rate results in smaller residence time and therefore small extent of reaction that will cause the hydrogen conversion to be smaller (Fig. 4). A decrease in the ratio of CO_2/CH_4 causes the water gas shift reaction to increase resulting in an increase in the conversion of hydrogen.

Fig. 5 shows that an increase in the ratio of H_2O/CH_4 causes an increase in reforming and this causes an increase in hydrogen conversion. On the other hand, a decrease in the ratio of H_2/CH_4 increases reforming and this causes hydrogen conversion to increase. A decrease in the ratio of CO/CH_4 increases the reverse water gas shift reaction, therefore causing a decrease in hydrogen.

As for the conversion of CH_4, Fig. 6 shows that the conversion of methane increases with the distance as it is consumed along the tubes. A decrease in the inlet temperature causes less reforming and therefore a decrease in conversion of methane relative to the base

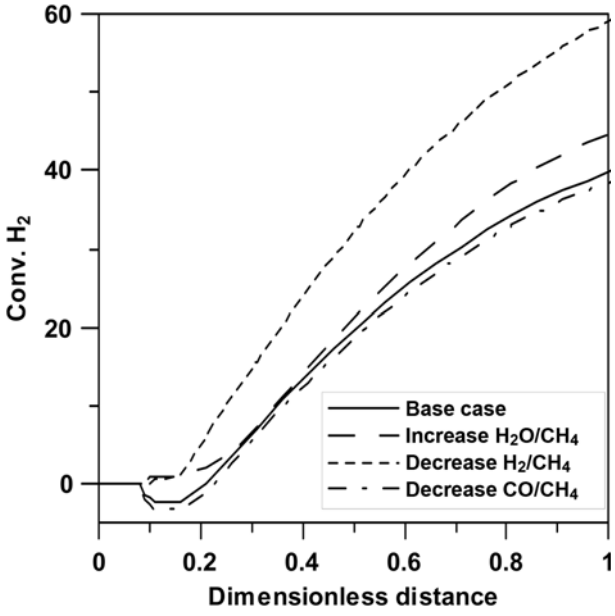

Fig. 5. Variations of hydrogen conversion and effect of some operating parameters.

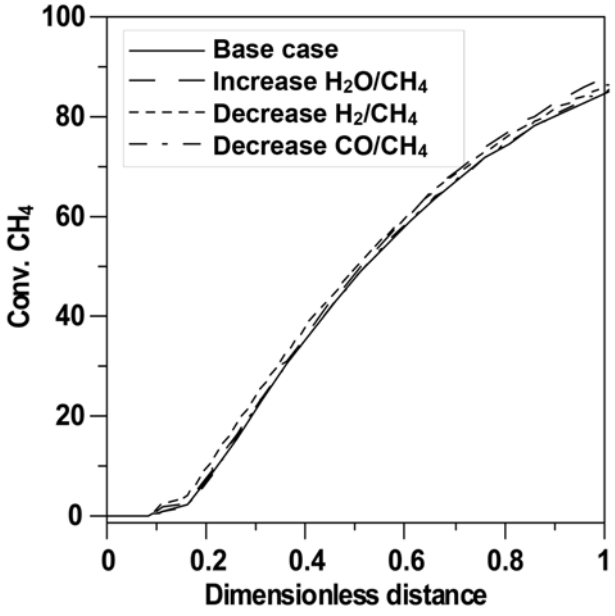

Fig. 7. Variations of methane conversion and effect of some operating parameters.

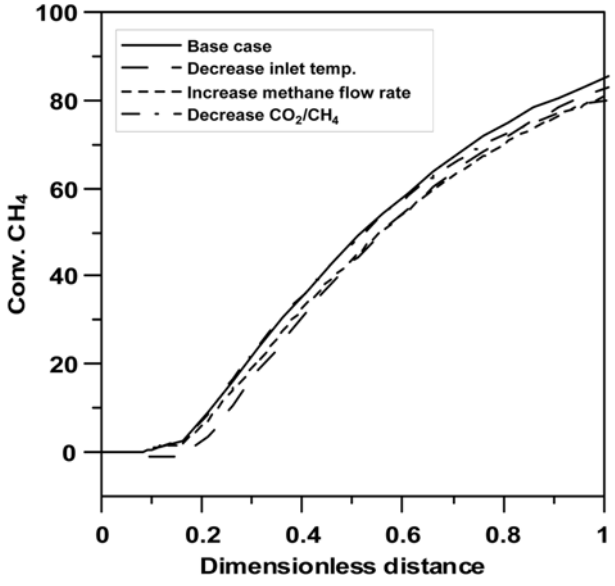

Fig. 6. Variations of methane conversion and effect of some operating parameters.

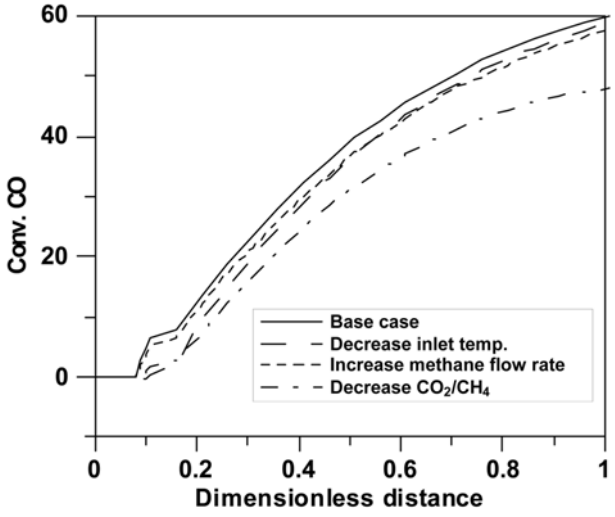

Fig. 8. Variations of carbon monoxide conversion and effect of some operating parameters.

case. The increase in the methane flow rate causes less reforming and leads to a decrease in methane conversion compared with the base case. The decrease in the ratio of CO_2/CH_4 results in less dry reforming, and therefore the value of methane conversion decreases relative to the base case. Fig. 7 shows that the increase in the ratio of H_2O/CH_4 increases the reforming and therefore increases the conversion of CH_4, while the decrease in the ratio of H_2/CH_4 causes more reforming and also leads to an increase in CH_4 conversion. Finally, a decrease in the ratio of CO/CH_4 results in more reforming and this causes an increase in methane conversion.

Similar to hydrogen, Figs. 8-9 show an increase in the conversion of carbon monoxide with distance. A decrease in the inlet temperature causes less reforming and thus less conversion of CO. An increase in methane flow rate results in smaller residence time, and therefore less conversion of CO. Unlike hydrogen, a decrease in the ratio of CO_2/CH_4 decreases the CO conversion because of less reforming. Fig. 9 shows that the increase in H_2O/CH_4 increases the conversion of CO because of the increase in reforming. A decrease in H_2/CH_4 causes a decrease in the conversion of CO because some of the CO produced in the reforming is consumed in the water gas shift reaction. Finally, a decrease in the ratio CO/CH_4 causes evidently an increase in CO conversion because of more reforming.

CONCLUSIONS

A first principle mathematical model was developed for a reform-

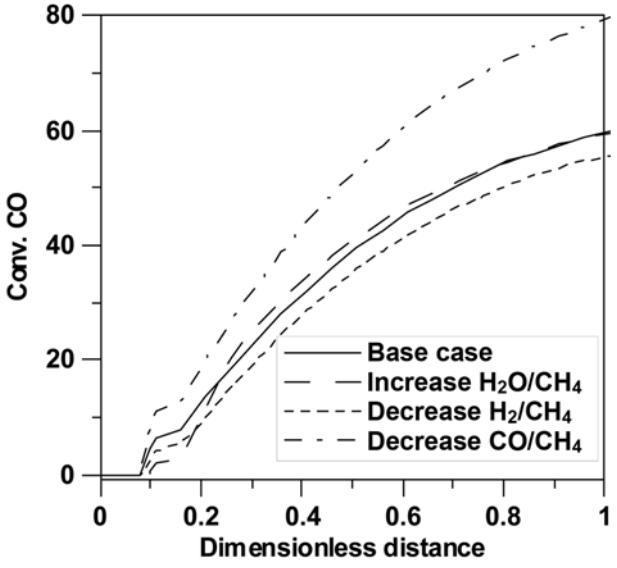

Fig. 9. Variations of carbon monoxide conversion and effect of some operating parameters.

er used in the Midrex direct reduction plant. A steady state, one-dimensional model with negligible axial dispersion was adopted for the catalyst tubes. The furnace was, on the other hand, modeled with bottom firing configuration. Satisfactory results were obtained when the model was validated against temperature and dry gas mole fractions, the only data available from a local iron/steel plant. The model was solved using the orthogonal collocation method for the base case to obtain local profiles of temperature and conversions, and was subsequently used for a sensitivity analysis of the effect of reactor operating parameters. Simulations were carried out to predict the reformer performance for variations in the inlet temperature, methane flow rate and ratios of H_2O, H_2, CO_2, CO to methane. The results obtained from the sensitivity analysis may be helpful in further optimization studies of the unit.

ACKNOWLEDGEMENT

This work was made possible by a generous grant from the National Plan for Science and Technology (Project # 08-ENE337-2) of Saudi Arabia.

NOMENCLATURE

A : reformer tube cross sectional area [m^2]
a_r : refractory furnace area to furnace free volume half ratio [m^{-1}]
a_t : tube side furnace area to furnace free volume half ratio [m^{-1}]
C_p : heat capacity of process gas [KJ/Kg K]
C_g : heat capacity of flue gas [KJ/Kg K]
d_p : center to center distance between catalyst particle diameter [m]
dt_i : internal diameters of the reformer tubes [m]
E_1 : grey gas component heat gas flux [W/m^2]
E_2 : clear gas component heat gas flux [W/m^2]
E_g : gas emissive powers in side fired furnaces [$J/m^2 \cdot hr$]
E_t : tube emissive powers in side fired furnaces [$J/m^2 \cdot hr$]
f : friction factor
F : fraction of fuel burned along the reformer
$n_{i,f}$: molar flow rate of gas i in the feed (i=H_2, CH_4, CO, CO_2, H_2O) [Kmol/hr]
G : process gas mass velocity [$Kg/hr \cdot m^2$]
G_g : process flue gas mass velocity [$Kg/hr \cdot m^2$]
K_1, K_2 : equilibrium constant for reaction 1, 2 [bar^2]
k_1, k_3 : rate coefficient of reaction 1, 3 respectively [Kmol·bar/ Kgcat·hr]
k_2 : rate coefficient of reaction 2 [Kmol/Kg-cat·hr·bar]
k_i : adsorption constants for (i=CH_4, CO and H_2) [bar^{-1}]
k_{H_2O} : dissociative adsorption constant for H_2O
L : reformer tube heated length [m]
l : coordinate [m]
l_c : characteristic length of pellets [m]
n_i : number of moles of component i in the reacting mixture [Kmol/hr]
P_i : partial pressure of component *i* in the gas bulk [bar]
$P_{i,c}$: partial pressure of component *i* at the center of the particle [bar]
$P_{i,p}$: partial pressure of component i at any position inside the particle [bar]
$P_{i,s}$: partial pressure of component i on catalyst particle surface [bar]
Q_r : net heat release rate [Kcal/hr]
r_i : rates of reactions (i=1, 2 and 3) [Kmol/Kgcat·hr]
R : ideal gas constant [KJ/Kmol·K]
T : temperature of the reacting mixture [K]
T_g : temperature of furnace gas [K]
T_s : temperature of inner tube skin [K]
T_r : refractory temperature [K]
V : free volume of reformer [m^3]

Greek Letters

ΔH_i : enthalpy change of reaction i [Kcal/mol]
ε_g : emissivity of the flue gas
ε_r : emissivity of refractory slab
ε_t : emissivity of tube wall
η_i : effectiveness factors associated with component i
ρ_g : process gas density [Kg/m^3]
ρ_θ : catalyst bed bulk density [Kg/m^3]
σ : Stefan-Boltzmann constant
ω : dimensionless coordinate of the catalyst pellet
ψ : band radiation fraction

REFERENCES

1. Midrex, Inc., http://www.midrex.com/.
2. F. Farhadi, M. Y. M. Hashemi and M. B. Babaheidari, *Ironmak. Steelmak.*, **30**, 18 (2003).
3. F. Farhadi, M. B. Babaheidari and M. M. Y. Hashemi, *Appl. Therm. Eng.*, **25**, 2398 (2005).
4. M. Sadri, K. Vakhshouri and M. M. Y. M. Hashemi, *Ironmak. Steelmak.*, **34**, 115 (2007).
5. J. Shayegan, M. M. Y. Hashemi and K. Vakhshouri, *Can. J. Chem. Eng.*, **86**, 757 (2008).
6. M. H. Hyman, *Hydrocarb. Process.*, **49**, 131 (1968).

7. J. Xu and G. F. Froment, *AIChE J.*, **35**, (1969).
8. J. C. De Deken, E. F. Devos and G. F. Froment, *Steam reforming of natural gas: Intrinsic kinetics, diffusional influences, and reactor design*, Chemical Reaction Engineering, ACS Symp. Ser., 196, Boston (1982).
9. J. R. Rostrup-Nielsen, *J. Catal.*, **85**, 31 (1984).
10. M. A. Soliman, S. El-Nashaie, A. Al-Obaid and I. Idriss, *Chem. Eng. Sci.*, **43**, 1801 (1988).
11. K. Ravi, Y. K. Joshi and B. K. Guha, *Chem. Eng. Technol.*, **12**, 358 (1989).
12. S. El-Nashaie, A. Idriss, M. A. Soliman and A. Al-Ubaid, *Can. J. Chem. Eng.*, **70**, 786 (1992).
13. H. M. Kvamsdal, H. F. Svendsen and O. Olsvik, *Chem. Eng. Sci.*, **54**, 2697 (1999).
14. J. K. Rajesh, S. K. Gupta and A. K. Ray, *Ind. Eng. Chem. Res.*, **39**, 706 (2000).
15. M. N. Pedenera, J. Pina, D. O. Borio and V. Bucala, *Chem. Eng. J.*, **94**, 29 (2003).
16. A. G. Dixon, M. Nijemeisland and E. H. Stitt, *Ind. Eng. Chem. Res.*, **44**, 6342 (2005).
17. S.-K. Jeon, C.-S. Park, S.-D. Kim, B.-H Song and J. M. Norbeck, *Korean J. Chem. Eng.*, **25**, 1279 (2008).
18. F. C. Roesler, *Chem. Eng. Sci.*, **22**, 1325 (1967).
19. C. McGreavy and M. Newman, IEEE Conf. on the Ind. Appl. of Dynamic Modelling, Durham., Sep. (1964).
20. C. P. P. Singh and D. N. Saraf, *Ind. Eng. Chem. Proc. Des. Dev.*, **18**, 1 (1979).
21. C. V. S. Murty and M. V. K. Murthy, *Ind. Eng. Chem. Res.*, **27**, 1832 (1988).
22. N. Selcuk, R. G. Siddal and J. M. Beer, *J. Inst. Fuel.*, **48**, 89 (1975).
23. W. W. Akers and D. P. Camp, *AIChE J.*, **4**, 471 (1955).
24. G. F. Froment and L. B. Bischoff, *Chemical reactor: Analysis and design*, John Wiley & Sons (1990).
25. R. Reid and T. Sherwood. *The Properties of gases and liquids*, McGraw Hill (1958).
26. M. Filla, *Chem. Eng. Sci.*, **39**, 159 (1984).
27. M. A. Soliman, *Chem. Eng. Sci.*, **43**, 1198 (1988).